GEOPHYSICAL RESEARCH LETTERS, VOL. 40, 60–65, doi:10.1029/2012GL054209, 2013

Earthquake source parameters from GPS-measured static displacements with potential for real-time application

Thomas B. O'Toole,[1] Andrew P. Valentine,[2] and John H. Woodhouse[1]

Received 24 November 2012; revised 16 October 2012; accepted 20 November 2012; published 16 January 2013.

[1] We describe a method for determining an optimal centroid–moment tensor solution of an earthquake from a set of static displacements measured using a network of Global Positioning System receivers. Using static displacements observed after the 4 April 2010, M_W 7.2 El Mayor-Cucapah, Mexico, earthquake, we perform an iterative inversion to obtain the source mechanism and location, which minimize the least-squares difference between data and synthetics. The efficiency of our algorithm for forward modeling static displacements in a layered elastic medium allows the inversion to be performed in real-time on a single processor without the need for precomputed libraries of excitation kernels; we present simulated real-time results for the El Mayor-Cucapah earthquake. The only a priori information that our inversion scheme needs is a crustal model and approximate source location, so the method proposed here may represent an improvement on existing early warning approaches that rely on foreknowledge of fault locations and geometries. **Citation:** O'Toole, T. B., A. P. Valentine, and J. H. Woodhouse (2013), Earthquake source parameters from GPS-measured static displacements with potential for real-time application, *Geophys. Res. Lett.*, *40*, 60–65, doi:10.1029/2012GL054209.

1. Introduction

[2] The ongoing growth and improvement of Global Positioning System (GPS) networks deployed in tectonically active regions has resulted in a considerable increase in the quantity and quality of GPS-derived observations of seismic deformation fields: data that are of great value in earthquake source studies. Recently, *O'Toole et al*. [2012] showed that high-rate GPS waveforms can be inverted using the centroid–moment tensor (CMT) algorithm of *Dziewonski et al*. [1981], allowing an optimal point source description of an earthquake to be determined from these time series. In principle, this adapted CMT method could also be applied to more widely available GPS-measured static displacement data, as we investigate in the present work.

[3] Such an undertaking is of interest in the context of earthquake early warning, because near-field geodetic measurements allow rapid magnitude determination and the construction of slip models in the minutes following an earthquake [e.g., *Blewitt et al*., 2006, 2009; *Allen and Ziv*, 2011; *Crowell et al*., 2012; *Wright et al*., 2012]. To make such inversions tractable in real-time, the fault's location and orientation are commonly assumed a priori using catalogues of known active faults, thus rendering the inverse problem linear. Because such information may be ambiguous, erroneous, or lacking, and earthquakes can occur on previously unidentified faults, an alternative approach is to construct a fault plane from the best point source recovered from the same geodetic data set. *Crowell et al*. [2012] found that aspects such as the total moment, location of peak slip, and slip extent obtained in source inversions using fault geometries taken from fault catalogues and moment tensor inversions are, broadly speaking, comparable. Consequently, there is great potential value in determining moment tensors from static displacement data for earthquake early warning, as it eliminates the need for a priori knowledge of the style of faulting in a particular area.

[4] Although geodetic source inversions assuming a finite fault are now routinely carried out, we are aware of only one previous study that performed inversions of static displacement data for an earthquake's CMT parameters [*Melgar et al*., 2011]. Using a precomputed library of excitation kernels, they performed a series of inversions on a grid of points distributed in space, choosing the location and moment tensor that yield the lowest data misfit as their CMT solution. The method proposed here is an alternative to that of *Melgar et al*. [2011], the main differences being that we solve directly for the centroid position without restriction to a grid, and our forward modeling method is efficient enough that all necessary computations are performed on-the-fly, allowing a priori assumptions about possible earthquake locations to be minimized. All that we require to perform an inversion is a static displacement data set, a crustal model, and an initial estimate of the source location from which we iterate to find the centroid position and moment tensor that best explain the data. In this paper, we perform source inversions using static displacements observed by GPS receivers of the California Real Time Network (CRTN) for the 2010 M_W 7.2 El Mayor-Cucapah, Mexico, earthquake. We introduce damping of the centroid location update into our iterative scheme to ensure that the inversion converges stably and demonstrate the potential of this new method by performing a CMT inversion of the El Mayor-Cucapah static displacement data set in simulated real-time.

2. Source Inversion Method

[5] A seismic point source can be represented by the vector $\mathbf{f}=(\mathbf{m},\mathbf{x})^T$, where $\mathbf{m}$ contains the six independent elements of the moment tensor and $\mathbf{x}$ contains the centroid

[1]Department of Earth Sciences, University of Oxford, Oxford, UK.
[2]Department of Earth Sciences, Universiteit Utrecht, Utrecht, The Netherlands.

Corresponding author: T. B. O'Toole, Department of Earth Sciences, University of Oxford, Oxford OX1 3AN, UK. (thomas.otoole@earth.ox.ac.uk)

0094-8276/13/2012GL054209

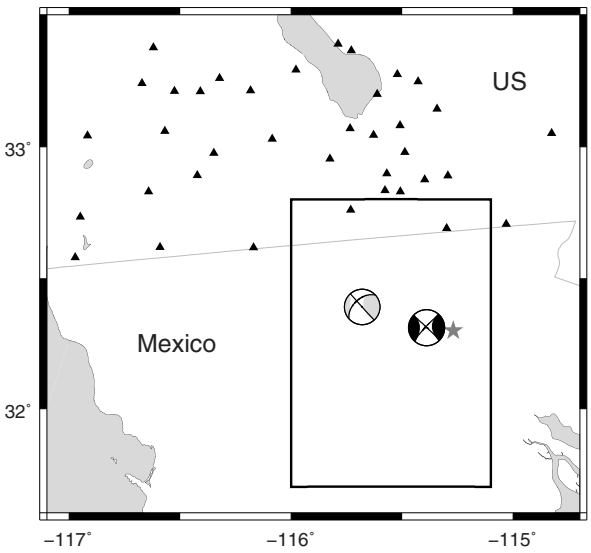

Figure 1. Distribution of CRTN GPS receivers (triangles) used in this study. Red star, the hypocenter of the 4 April 2010, M_W 7.2 El Mayor-Cucapah earthquake taken from the U.S. Geological Survey PDE catalogue. Black and green beach balls, CMT solutions from the Global CMT catalogue (www.globalcmt.org) and *Melgar et al*. [2011], respectively. Rectangle, the area enlarged in Figure 2a.

coordinates in space and time. We seek to determine **f** from a set of seismic observations **d**. Conventionally, this data set has consisted of long-period teleseismic waveforms [e.g., *Dziewonski et al*., 1981, 1983; *Dziewonski and Woodhouse*, 1983], although regional seismograms and near-field high-rate GPS time series have also been used [e.g., *Pondrelli et al*., 2002; *O'Toole et al*., 2012]. Here, our data are GPS-measured static displacements; each element of **d** represents one component of the static displacement field measured at a particular location. Such data are independent of time; thus, **x** contains only the latitude, longitude, and depth of the centroid in the present case.

[6] If we assume that **x** is known, then the inverse problem for the moment tensor is linear [*Gilbert*, 1973], with a least-squares solution given by [e.g., *Menke*, 1989]

$$\mathbf{m} = \left(\mathbf{A^T A}\right)^{-1}\mathbf{A^T d}, \tag{1}$$

where the matrix **A** contains the excitation kernels $\partial s/\partial m_i$. These are the static displacements excited by unit sources given by each component of the moment tensor, corresponding to each element of the data vector. We calculate the excitation kernels in a plane-layered elastic medium using the propagator algorithm described by *O'Toole and Woodhouse* [2011], which implements the minor vector theory of *Woodhouse* [1980] to compute displacement spectra stably and efficiently at any frequency including 0 Hz.

[7] In general, the centroid location is not known a priori, so ideally we should attempt to recover the earthquake's location parameters along with the moment tensor in any inversion. One approach to solving this nonlinear inverse problem is to perform a series of inversions on a grid of possible source locations using equation (1); the moment tensor and location that best explains the observed static displacement data is then an approximation of the true solution [*Melgar et al*., 2011]. Alternatively, we can recover the optimum centroid location and moment tensor simultaneously by linearizing the problem and applying the iterative scheme

$$\mathbf{f}_{i+1} = \mathbf{f}_i + \left(\mathbf{A}_i^T\mathbf{A}_i\right)^{-1}\mathbf{A}_i^T\mathbf{e}, \tag{2}$$

where $\mathbf{e} = \mathbf{d} - \mathbf{s}_i$ is the difference between the observed data and the synthetic data **s**. Matrix **A** now also includes the location kernels $\partial s/\partial x_i$, the partial derivatives of the synthetic static displacements with respect to the centroid location and depth, which are calculated as described by *O'Toole et al*. [2012]. The terms in equation (2) with subscripts depend on **f** and so must be recalculated at each iteration. The initial source $\mathbf{f}_0$ is typically the result of a moment tensor inversion via equation (1) fixed at a location obtained from, for example, *P* wave arrival times. Because we are examining earthquake sources, which should have no explosive component, we constrain the trace of the moment tensor to equal zero in the following.

3. El Mayor-Cucapah Earthquake

[8] The 4 April 2010, M_W 7.2 El Mayor-Cucapah, Mexico, earthquake was recorded by 105 CRTN GPS receivers located throughout southern California. The raw GPS data were processed using the method of instantaneous positioning, a network-based approach that allows precise and accurate real-time positioning (relative to a known, fixed station) from a single epoch of GPS data [*Bock et al*., 2000] and made available to the community, along with the resulting 1 Hz GPS time series, as described by *Bock et al*. [2011]. Here, we apply the algorithm presented by *Allen and Ziv* [2011] to extract static displacements from these GPS waveforms. We use the final set of estimates from 37 stations (Figure 1, triangles) to investigate whether we can apply the foregoing theory to perform source inversions using these data. We invert only the horizontal component static displacements because the amplitudes of vertical offsets excited in this earthquake are comparable with their measurement uncertainties.

[9] Previously, *Melgar et al*. [2011] used a similar static displacement data set to determine a CMT solution for this event. Their solution (Figure 1, green beach ball) provides a useful benchmark to compare with our results. The starting location for our source inversion is taken from the U.S. Geological Survey Preliminary Determination of Epicenters (PDE) catalogue (Figure 1, red star). We compute derivative kernels using the same layered crustal model as *Melgar et al*. [2011] and apply the iterative inversion scheme given in equation (2) to recover a CMT solution for this event. It is well known that the $M_{r\theta}$ and $M_{r\phi}$ excitation kernels vanish as the source approaches the free surface; hence, these components of the moment tensor cannot be reliably determined for shallow earthquakes [e.g., *Kanamori and Given*, 1981]. Consequently, we must impose a limit on the shallowest depth that is allowed to be recovered during the inversion. If the inversion tries to move the centroid depth shallower than 4 km, we fix the event depth to this value in subsequent iterations and no longer solve for this parameter. A similar approach is taken in Global CMT inversions, although depths are typically fixed slightly deeper at 12 km; the threshold depth used here is chosen in an effort to maintain comparability of our solution with that of *Melgar et al*. [2011], which has a depth of 4 km.

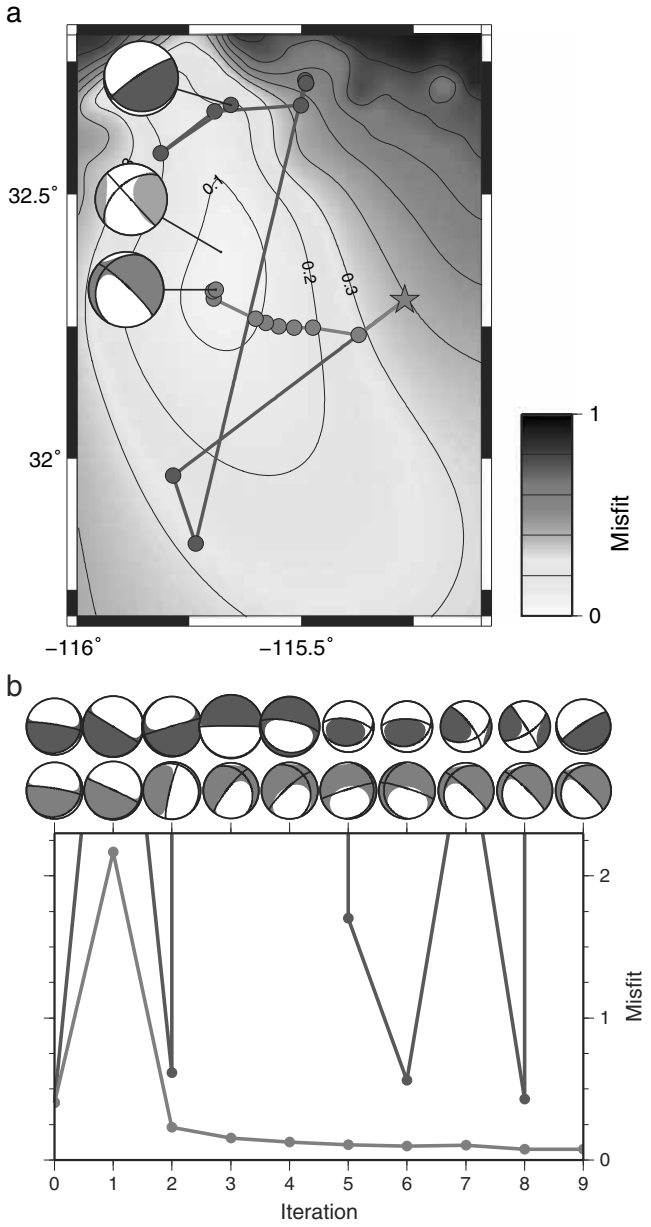

Figure 2. The evolution of centroid location (a) and misfit (b) over 10 iterations of our source inversion algorithm before (blue) and after (red) the introduction of location step-length damping. Green beach ball, the solution of *Melgar et al*. [2011]. Our inversions start at the PDE hypocenter (red star). Contours and shading denote the value of the misfit function at a depth of 4 km.

[10] The evolution of the source location over 10 iterations of the inversion algorithm is shown by the blue line in Figure 2a; large changes in centroid location are apparent from one iteration to the next. Because the inversion immediately moves the source to the shallowest permitted depth (4 km), the misfit function at this depth, calculated by performing a series of moment tensor inversions on a grid of points, is also shown by the shaded contour map. The inversion algorithm should move the centroid downhill on this misfit surface toward the global minimum. Clearly, the inversion fails to behave in this way; the actual evolution of the misfit over the iterative inversion is shown by the blue line in Figure 2b. The large oscillations in misfit between iterations confirm that the attempted inversion of static displacement data is unstable and goes beyond the limit of our linear approximation's validity.

[11] The failure of the linearization is apparent in the great disparity between the misfit of each source output by the inversion (Figure 2b, blue line) and the true minimum misfit value at each location visited during the inversion, which is given by the misfit surface in Figure 2a. The large changes in source location mean that the moment tensor output by the inversion is a very poor approximation of the actual best moment tensor at the new location; hence, the misfit function over the 10 iterations is poorly behaved. To stabilize the inversion, it is therefore necessary to adapt the iterative scheme so that the change in source location allowed in any one iteration is restricted.

4. Location Step-Length Damping

[12] The inversion of static displacement data attempted in the previous section indicates that nonlinearity in the relationship between data and source parameters, particularly the centroid location, causes instabilities leading to unrealistically large location updates. To counteract this problem, we wish to limit the size of the location change permissible on any given iteration. By a process similar to Gaussian elimination, we rewrite equation (2) as two coupled equations:

$$\mathbf{x}_{i+1} = \mathbf{x}_i + \eta\left[\mathbf{B}^T\mathbf{B} - \mathbf{B}^T\mathbf{A}\left(\mathbf{A}^T\mathbf{A}\right)^{-1}\mathbf{A}^T\mathbf{B}\right]^{-1}\left[\mathbf{B}^T\mathbf{e} - \mathbf{B}^T\mathbf{A}\left(\mathbf{A}^T\mathbf{A}\right)^{-1}\mathbf{A}^T\mathbf{e}\right] \quad (3)$$

$$\mathbf{m}_{i+1} = \mathbf{m}_i + \left(\mathbf{A}^T\mathbf{A}\right)^{-1}\left[\mathbf{A}^T\mathbf{e} - \mathbf{A}^T\mathbf{B}(\mathbf{x}_{i+1} - \mathbf{x}_i)\right] \quad (4)$$

where $\mathbf{A} = \partial s/\partial m_i$ contains the excitation kernels and $\mathbf{B} = \partial s/\partial x_i$ the location kernels. When $\eta = 1$, this form is exactly equivalent to equation (2). Setting $\eta < 1$, however, allows us to damp the location update from one iteration to the next, and we can use the true, restricted $\mathbf{x}_{i+1}$ in equation (4) to obtain a self-consistent set of source parameters. A similar approach has been used by a number of authors in the context of joint determination of earthquake source parameters and earth structure [*Pavlis and Booker*, 1980; *Morelli and Dziewonski*, 1991; *Valentine and Woodhouse*, 2010].

[13] We repeat the previous inversion, except that we now damp the location step-length heavily, choosing $\eta = 0.2$. In contrast to the earlier attempt, the centroid now moves smoothly downhill in misfit space to converge at the global minimum (Figure 2a, red line), suggesting that the damping we have introduced successfully stabilizes the inversion. The improved behavior of the damped inversion is also apparent in the evolution of the misfit during the inversion (Figure 2b, red line), which is a much better approximation of the true minimum misfit. Although the misfit increases after the first iteration, where the restricted location update is still large enough for the linearization to fail, the damping is sufficient that the solution is still close enough to the actual best solution at that location for the misfit to decrease on subsequent iterations and the inversion to converge. A consequence of applying damping is that convergence is slowed as the solution approaches the global minimum. To avoid this issue, we apply damping only when the

suggested location update is larger than some value over which we assume the linearization holds; here, this length is chosen as 10 km. For real-time inversions, where the amount of damping required is not known a priori, one could adopt this approach and set η to be conservatively small ($\eta = 0.1$, say). This would ensure stability of the inversion but also allows rapid convergence when the solution is close to the global minimum. For comparison, the CMT solution of *Melgar et al*. [2011] is also shown in Figure 2a (green beach ball). The misfit function plotted in Figure 2a is sufficiently well behaved that one could start a step-length damped inversion at any point, and it would converge to the global minimum. Although there is a local minimum visible at the northeast corner of this plot, this arises from the fact that there is a GPS station directly above this point, the data from which were used in the construction of the misfit function. In practice, one would ignore data from this station if the starting point for our iterative inversion was located nearby, and there would be no local minimum to potentially hamper the inversion.

[14] Although step-length damping clearly stabilizes the inversion, the final solution is physically unrealistic due to the large dip-slip components, which, despite our depth fixing, dominate the solution (see Table S1). To avoid this problem, we perform a further inversion where we impose the condition that $M_{r\theta} = M_{r\phi} = 0$. Although other forms of regularization could be applied, we employ this constraint as it is also used in Global CMT analyses of some earthquakes with centroid depths shallower than ~15 km. We find that introducing this constraint also helps to stabilize the inversion so that weaker step-length damping is required; source parameters output for a constrained inversion with $\eta = 0.5$ are shown in Table S1. When compared with the full moment tensor obtained previously, the solution with $M_{r\theta} = M_{r\phi} = 0$ explains the data almost as well while also having a much smaller norm and so could be preferred on the principle of parsimony.

5. Real-time Application

[15] The success of our modified source inversion scheme leads us to investigate whether this method could be applied to invert static displacement data in real-time. The exact setup of the real-time inversion described below is somewhat arbitrary, and we make no claim that the current scheme is ideal; rather, we merely hope to demonstrate that real-time inversion is possible without the need for precomputed libraries of excitation kernels or a priori knowledge of fault locations and geometries. The real-time static displacement data set is extracted from the 1 Hz GPS waveforms using the algorithm of *Allen and Ziv* [2011], which averages out dynamic displacements caused by the passage of seismic waves through each station, to produce an estimate of the static displacement field at the GPS receiver sampling rate, i.e., every 1 s for the El Mayor-Cucapah data set. Here, this approach returns a good approximation of the final static displacement as little as 7 s after a station first detects shaking, although the exact time will vary according to factors like the source–receiver distance and earthquake magnitude. Our inversion approach is much the same as before; we apply step-length damping with $\eta = 0.5$ along with the constraint that $M_{r\theta} = M_{r\phi} = 0$. The only difference is that we simulate a real-time application by refreshing the data vector at the end of each iteration so that it contains the most recent estimate of the static displacement field.

[16] In this experiment, the inversion begins when more than 20 data points become available. This is a somewhat arbitrary choice and may be adapted to suit particular circumstances. The inversion continues until the final set of static displacements is reported and the misfit falls below a predefined threshold. Alternatively, the inversion could run until there is no significant decrease in the misfit between iterations or the change in the model is very small from one iteration to the next; these stopping conditions may be more suitable for a real-time implementation than the simple misfit threshold currently used. Here, the inversion is triggered 61 s after the PDE catalogue origin time. The final solution, which is essentially identical to that given in Table S1, is available 82 s later (all run times quoted in this report are for a single 2.4 GHz processor).

[17] The results of the real-time inversion are summarized in Figure 3. Unlike inversions that use precomputed libraries of excitation kernels or model the crust as a homogeneous half-space, each iteration of our inversion takes longer than 1 s, so we do not produce a solution for every set of static displacement estimates. However, the time at which our final solution is available is comparable with that of *Melgar et al*. [2011]; this time is mainly controlled by when the data are representative of the final static offsets and not how long it takes to do an iteration of the inversion. The duration of an iteration depends most strongly on the number of data points used and so increases as more stations start reporting static displacements, peaking at ~16 s when data from all 37 stations are available. The first iteration moves the centroid ~30 km westward and produces a marked decrease in misfit. The misfit does not change significantly on subsequent iterations, although it is calculated with respect to the updated data set rather than just the data used in that iteration. This behavior indicates that each solution must explain the new data added after that iteration reasonably well. The moment magnitude of our solution decreases towards the Global CMT value of M_W 7.2 as the centroid moves northward and closer to the network.

[18] Solutions from a selected number of iterations are shown on the map in Figure 3, and are annotated with the time that they are available, in units of seconds after the earthquake began. The advantage of performing an inversion in real-time, rather than waiting for the final static displacement data set to be available, is that the early iterations allow the centroid to move close to its true final position, so that convergence is very rapid once all the data are available. Observed and synthetic static displacements computed for our final source are also shown; the level of agreement reflects the low misfit value of this inversion.

6. Concluding Remarks

[19] Our source inversion of real-time static displacements for the El Mayor-Cucapah earthquake shows that the method developed in this paper may be useful for determining the location, magnitude, and style of faulting in the context of earthquake early warning. Ideally, the GPS network would provide complete azimuthal coverage of the source, allowing the radiation pattern to be fully sampled. Here, all stations lie north of the event, so this study represents something of a worst-case scenario. The fact that our step-length damped

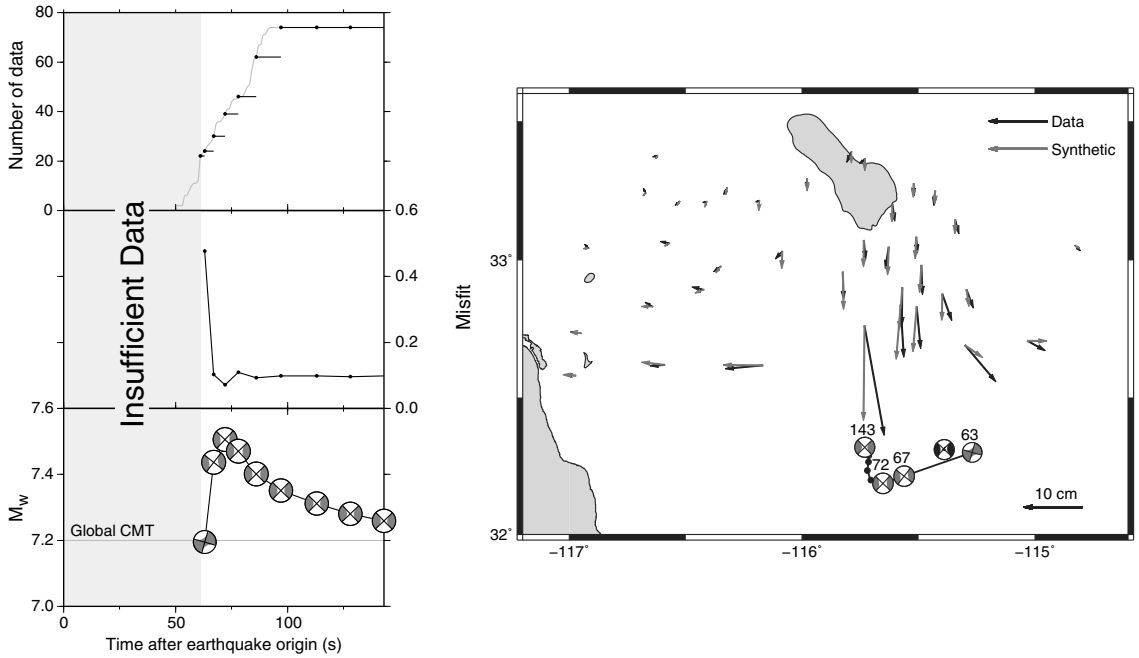

Figure 3. Results of a simulated real-time source inversion of static displacement data for the El Mayor-Cucapah earthquake. Top left, amount of data available as a function of time (gray line). Black tadpoles, the amount of data used in, and duration of, each iteration of our inversion. Middle left, evolution of misfit as function of time. Bottom left, source mechanism and moment magnitude output by the inversion over time. Gray line, the Global CMT magnitude. Right, map showing the fit between horizontal static displacement data (black arrows) and synthetics (red arrows) for our final solution. A selection of the CMT solutions produced during the real-time inversion are also plotted; the number above each beach ball indicates the time (in seconds after the earthquake origin time) at which that solution is available using a single 2.4 GHz processor. Black beach ball, the Global CMT solution.

inversion converges even in this situation indicates that our algorithm is robust with respect to network geometry. This result is important in the context of monitoring subduction zone events, where land-based real-time GPS networks are necessarily one-sided. Because our inversion approach aims to minimize the amount of a priori information required, it is amenable to automation. In addition to the data, all that we need to perform an inversion is a preliminary hypocenter, which can be obtained within a few seconds of the detection of wave arrivals using existing seismic or geodetic early warning systems [e.g., *Allen et al*., 2009; *Crowell et al*., 2009], and a crustal model, which, in the absence of better knowledge of the local earth structure, can be taken from an appropriate global model, such as Crust 2.0 (http://igppweb.ucsd.edu/~gabi/rem.html). No assumptions about possible fault locations and geometries need be made, nor do we require any knowledge of preexisting faults in the area. Furthermore, we demonstrate that it is possible to obtain a CMT solution rapidly without the need for large precomputed databases of excitation kernels. The efficiency of our forward modeling method is such that all of the requisite derivative kernels can be calculated on-the-fly using a standard workstation with a single 2.4 GHz processor, even when a layered crustal model is used. As a consequence, our inversion method may be useful in improving the resilience of earthquake early warning systems, because it is flexible enough to cope with earthquakes occurring in unexpected locations. Given the average density of receivers in modern geodetic networks like CRTN, along with typical GPS measurement uncertainties, we expect that earthquakes with $M_W \geq 6.0$ will have sufficiently high signal-to-noise ratios to be analyzed with the algorithm proposed here. Of course, this magnitude threshold will vary spatially within a network depending on the proximity of the centroid to subsets of receivers and is also partly controlled by the source mechanism due to the relatively large uncertainties in vertical displacement measurements made using GPS [e.g., *Langbein and Bock*, 2004]. It should also be noted that our assumption of a point source breaks down for near-field static displacements measured during the largest seismic events such as the 2011 M_W 9.1 Tohoku earthquake. These great ruptures may be treated more appropriately using finite fault inversions. *Amoruso et al*. [2004] and *Hearn and Bürgmann* [2005] showed that it is important to account for the effect of crustal layering in inversions of static displacement data, and the present work raises the possibility that Green's functions calculated in layered elastic media could also be computed in real-time for use in rapid slip inversions, in addition to the CMT-style analyses presented here. Because measurement uncertainties in GPS positions have been well studied [e.g., *Langbein and Bock*, 2004], in the future, the inversion scheme could be reformulated to incorporate this information; such an undertaking would allow the vertical displacement data to be included and enable quantification of uncertainties in recovered model parameters.

[20] In addition to earthquake early warning, the method developed in this paper can be used to determine candidate fault planes for the purpose of finite fault slip inversions both in real-time and after the event. Furthermore, because our inversion approach mirrors that of the CMT algorithm, the present work should enable near- and far-field data to be

combined and reconciled in a single inverse problem, with the potential for quantifying and reducing errors in CMT solutions. Although we have focused on using GPS-measured static displacement data to obtain the first-order information about an earthquake, line-of-sight displacements measured using synthetic aperture radar interferometry could also be used.

[21] **Acknowledgements.** We thank Richard Allen for providing the output of his real-time static displacement picking algorithm for the El Mayor-Cucapah earthquake. The GPS displacement waveforms from which the data used in this report were derived are a product of the NASA Advanced Information Systems Technology project (grant NNX09AI67G) at Scripps, JPL, and Caltech and were obtained from the Southern California Earthquake Data Center (http://www.data.scec.org/research/MayorCucapah20100404/). We thank the reviewers Tim Wright, Yehuda Bock, and Guoquan Wang for their comments, which helped improve the original manuscript. T.B.O.'T. is supported by the UK Natural Environment Research Council under grant NE/H527791/1. A.P.V. is supported by the Netherlands Organisation for Scientific Research through TOP-subsidie 854.10.002. Computational facilities are supported under grant NE/B505997/1.

References

Allen, R. M., and A. Ziv (2011), Application of real-time GPS to earthquake early warning, *Geophys. Res. Lett.*, *38*, L16310, doi:10.1029/2011GL047947.

Allen, R. M., P. Gasparini, O. Kamigaichi, and M. Böse (2009), The status of earthquake early warning around the world: An introductory overview, *Seismol. Res. Lett.*, *80*(5), 682–693, doi:10.1785/gssrl.80.5.682.

Amoruso, A., L. Crescentini, and C. Fidani (2004), Effects of crustal layering on source parameter inversion from coseismic geodetic data, *Geophys. J. Int.*, *159*, 353–364, doi:10.1111/j.1365-246X.2004.02389.x

Blewitt, G., C. Kreemer, W. C. Hammond, H.-P. Plag, S. Stein, and E. Okal (2006), Rapid determination of earthquake magnitude using GPS for tsunami warning systems, *Geophys. Res. Lett.*, *33*, L11309, doi:10.1029/2006GL026145.

Blewitt, G., W. C. Hammond, C. Kreemer, H.-P. Plag, S. Stein, and E. Okal (2009), GPS for real-time earthquake source determination and tsunami warning systems, *J. Geod.*, *83*, 335–343, doi:10.1007/s00190-008-0262-5.

Bock, Y., R. M. Nikolaidis, P. J. de Jonge, and M. Bevis (2000), Instantaneous geodetic positioning at medium distances with the Global Positioning System, *J. Geophys. Res.*, *105*(B12), 28,223–28,253, doi:10.1029/2000JB900268.

Bock, Y., D. Melgar, and B. W. Crowell (2011), Real-time strong-motion broadband displacements from collocated GPS and accelerometers, *Bull. Seismol. Soc. Am.*, *101*(6), 2904–2925, doi:10.1785/0120110007.

Crowell, B. W., Y. Bock, and M. B. Squibb (2009), Demonstration of earthquake early warning using total displacement waveforms from real-time GPS networks, *Seismol. Res. Lett.*, *80*(5), 772-782, doi:10.1785/gssrl.80.5.772.

Crowell, B. W., Y. Bock, and D. Melgar (2012), Real-time inversion of GPS data for finite fault modeling and rapid hazard assessment, *Geophys. Res. Lett.*, *39*, L09305, doi:10.1029/2012GL051318.

Dziewonski, A. M., and J. H. Woodhouse (1983), An experiment in systematic study of global seismicity: centroid-moment tensor solutions for 201 moderate and large earthquakes of 1981, *J. Geophys. Res.*, *88*(B4), 3247–3271, doi:10.1029/JB088iB04p03247.

Dziewonski, A. M., T.-A. Chou, and J. H. Woodhouse (1981), Determination of earthquake source parameters from waveform data for studies of global and regional seismicity, *J. Geophys. Res.*, *86*(B4), 2825–2852, doi:10.1029/JB086iB04p02825.

Dziewonski, A. M., A. Friedman, D. Giardini, and J. H. Woodhouse (1983), Global seismicity of 1982: centroid-moment tensor solutions for 308 earthquakes, *Phys. Earth Planet. Inter.*, *33*(2), 76–90, doi:10.1016/0031-9201(83)90141-3.

Gilbert, F. (1973), Derivation of source parameters from low-frequency spectra, *Philos. Trans. R. Soc., A*, *274*(1239), 369–371, doi:10.1098/rsta.1973.0065.

Hearn, E. H., and R. Bürgmann (2005), The effect of elastic layering on inversions of GPS data for coseismic slip and resulting stress changes: Strike-slip earthquakes, *Bull. Seismol. Soc. Am.*, *95*(5), 1637-1653, doi:10.1785/0120040158.

Kanamori, H., and J. W. Given (1981), Use of long-period surface waves for rapid determination of earthquake-source parameters, *Phys. Earth Planet. Inter.*, *27*, 8–31, doi:10.1016/0031-9201(81)90083-2.

Langbein, J., and Bock, Y. (2004), High-rate real-time GPS network at Parkfield: Utility for detecting fault slip and seismic displacements, *Geophys. Res. Lett.*, *31*, L15S20, doi:10.1029/2003GL019408.

Melgar, D., Y. Bock, and B. W. Crowell (2011), Real-time centroid moment tensor determination for large earthquakes from local and regional displacement records, *Geophys. J. Int.*, *188*, 703–718, doi:10.1111/j.1365-246X.2011.05297.x.

Menke, W. (1989), *Geophysical Data Analysis: Discrete Inverse Theory*, Academic Press, New York, 289 pp.

Morelli, A., and A. Dziewonski (1991), Joint determination of lateral heterogeneity and earthquake location, in *Glacial Isostasy*, Sea-Level and Mantle Rheology, edited by R. Sabadini, K. Lambeck, and E. Boschi, pp. 515–534, Kluwer Academic Publishers, Dordrecht.

O'Toole, T. B., and J. H. Woodhouse (2011), Numerically stable computation of complete synthetic seismograms including the static displacement in plane layered media, *Geophys. J. Int.*, *187*, 1516–1536, doi:10.1111/j.1365-246X.2011.05210.x.

O'Toole, T. B., A. P. Valentine, and J. H. Woodhouse (2012), Centroid–moment tensor inversions using high-rate GPS waveforms, *Geophys. J. Int.*, *191*, 257–270, doi:10.1111/j.1365-246X.2012.05608.x.

Pavlis, G., and J. Booker (1980), The mixed discrete-continuous inverse problem: Application to the simultaneous determination of earthquake hypocenters and velocity structure, *J. Geophys. Res.*, *85*, 4801–4810, doi:10.1029/JB085iB09p04801.

Pondrelli, S., A. Morelli, G. Ekström, S. Mazza, E. Boschi, and A. M. Dziewonski (2002), European–Mediterranean regional centroid–moment tensors : 1997–2000, *Phys. Earth Planet. Inter.*, *130*, 71–101, doi:10.1016/S0031-9201(01)00312-0.

Valentine, A. P., and J. H. Woodhouse (2010), Reducing errors in seismic tomography: combined inversion for sources and structure, *Geophys. J. Int.*, *180*, 847–857, doi:10.1111/j.1365-246X.2009.04452.x.

Woodhouse, J. (1980), Efficient and stable methods for performing seismic calculations in stratified media, in Physics of the Earth's Interior, Proceedings of the International School of Physics "Enrico Fermi", Course LXXVIII, pp. 127–151, North Holland, Amsterdam.

Wright, T. J., N. Houlié, M. Hildyard, and T. Iwabuchi (2012), Real-time, reliable magnitudes for large earthquakes from 1 Hz GPS precise point positioning: The 2011 Tohoku-Oki (Japan) earthquake, *Geophys. Res. Lett.*, *39*, L12302, doi:10.1029/2012GL051894.